Charge fluctuations and the tunneling spectra of non-magnetic metallic nanoparticles

Gustavo A. Narvaez and George Kirczenow
Department of Physics, Simon Fraser University, Burnaby, British Columbia, Canada, V5A 1S6
(February 1, 2008)

We present microscopic transport calculations of the tunneling spectra of non-magnetic metal nanoparticles. We show that charge fluctuations give rise to tunneling resonances of a new type. Positive and negative fluctuations have differing kinetics and thus account for previously unexplained spectral features that are found experimentally under only forward or only reverse applied bias. The observed clustering of tunneling resonances of Al nanoparticles arises naturally from our theory.

PACS numbers: 73.22.-f, 73.22.Dj

In metal particles with dimensions on the nanometer scale the electron de Broglie wavelength is comparable to the size of the particle. Thus these nanoparticles exhibit discrete electronic spectra that can be observed directly in tunneling measurements. [1] Such experiments have recently been carried out for Al, [2] Au, Ag, Cu [3] and Co [4] nanoparticles coated with aluminum oxide that forms the tunnel barrier. They have attracted considerable attention since they can in principle provide detailed microscopic information relevant to many important but poorly understood aspects of nanoscale metal physics that range from the effects of disorder and surface chemistry to nanoscale ferromagnetism and superconductivity. [1] Some of the observed effects have been modelled phenomenologically with considerable success. [5–9] However even in the case of Al nanoparticles (the simplest and most studied of these systems) the present understanding of the results of the experiments is far from satisfactory. For example, some of the tunneling resonances that are seen experimentally can be matched with similar features that are observed when the bias applied to the nanoparticle is reversed. Thus they can reasonably be attributed to tunneling through particular electronic states of the nanoparticle. [2] However, other observed tunneling resonances have no identifiable counterparts under reverse bias and their physical origin has remained a mystery. [2] This suggests that some important aspects of the physics of electron transport through the metal nanoparticles have not been recognized to date. In this Communication we identify a plausible candidate: We demonstrate theoretically that *charge fluctuations* that occur whenever a current flows through the nanoparticle should result in transport resonances of a new type that begin already *in the first step* of the Coulomb staircase. We predict that for most samples these new resonances (unlike other tunneling features) should be *much* stronger for one direction of the applied bias than for the other. Thus charge fluctuations account naturally for the presence in the experimental tunneling spectra of the previously unexplained resonances described above. We argue that in typical samples this new mechanism should account for a substantial fraction of all of the observed tunneling features.

We illustrate our predictions with numerical calculations for Al nanoparticles whose electronic structure is described by a microscopic tight-binding model [10] that incorporates the geometry of the particle and accounts for the presence of disorder as well as the detailed chemistry of the metal-oxide interface. Salient features of the electronic structure are depicted in Fig. 1 which shows the calculated energy eigenvalues E_i near the Fermi level E_F of a disc-shaped nanoparticle of volume $\mathcal{V} = 16.9nm^3$. The amplitudes of the electron eigenfunctions φ_i on the top (T) and bottom (B) surfaces of the nanoparticle are also displayed for selected electron eigenstates. The diameter of each circle represents the magnitude of φ_i at a given atomic site (indicated by the central dot). Due to the presence of surface disorder, the relief of the amplitude is quite complex and depends strongly on the electronic state that is considered and on which surface is shown.

The wavefunction landscapes at these surfaces enter the electron tunneling efficiencies γ_i^λ between level i of the nanoparticle and contact λ (=T,B) as follows: Let $M_{e,i}^\lambda$ be the tunneling matrix element between the electronic state $\Psi_e^\lambda(\vec{r}) = \langle\vec{r}|\Psi_e^\lambda\rangle$ of the contact and the state $\varphi_i(\vec{r}) = \langle\vec{r}|\varphi_i\rangle$ of the nanoparticle. Since $M_{e,i}^\lambda$ is a transfer matrix element we adopt the expression $M_{e,i}^\lambda = \mathcal{R}\int_{\Omega_\lambda} d\vec{S}\,\Psi_e^\lambda\varphi_i$ widely used in the quantum chemistry literature to calculate transfer matrix elements between different molecular states. [11] $\mathcal{R}$ is an energy scale factor and Ω_λ is the T or B surface of the nanoparticle. The nanoparticle electron wavefunction is $\varphi_i(\vec{r}) = \sum_{\vec{R}_j} a_{j,i}^\alpha\phi_\alpha(\vec{r}-\vec{R}_j)$ where the coefficients $a_{j,i}^\alpha$ arise from diagonalization of a tight-binding Hamiltonian constructed using a s, p, d orbital basis (ϕ_α). [10] Obtaining a realistic $\Psi_e^\lambda(\vec{r})$ in the contact/oxide region is difficult. However, we do not need the whole wavefunction but only the values that $\Psi_e^\lambda(\vec{r})$ takes at the surface of the nanoparticle. From a tight-binding point of view with only s orbitals in the basis, the wavefunction at the surface can be written $\Psi_e^{\Omega_\lambda}(\vec{r}) = \sum_{\vec{r}_j} b_{j,e}^s\phi_s(\vec{r}-\vec{r}_j)$ with $\vec{r}_j$ the positions of the atomic sites at Ω_λ. Due to the disordered nature of the metal-oxide interface and time reversal symmetry, we represent the coefficients $b_{j,e}^s$

by those arising from diagonalization of a matrix $\mathcal{M}$ of order $\mathcal{N}$ within the Gaussian Orthogonal Ensemble weighted by the WKB extinction coefficient $e^{-\kappa d_\lambda^{ox}}$. [12] $\mathcal{N}$ is the number of sites at surface Ω_λ, $\kappa = \sqrt{2mV_b/\hbar^2}$ and $V_b \simeq 1.2eV$ [13]; d_λ^{ox} is the thickness of the oxide barrier. We average over an ensemble of matrices $\mathcal{M}$ to model the fact that different lead states $|\Psi_e\rangle$ couple to a given nanoparticle state $|\varphi_i\rangle$. Thus we find

$$\gamma_i^\lambda = \frac{2\pi}{\hbar}\mathcal{R}^2\nu_\lambda(E_H)e^{-2\kappa d_\lambda^{ox}}\left\langle\left|\sum_{\vec{R}_j}\sum_\alpha [b_{j,e}^s a_{j,i}^\alpha]_\lambda\right|^2\right\rangle. \quad (1)$$

$\nu_\lambda(E_H)$ is the density of states at the highest occupied level in the lead λ and $\langle\cdots\rangle$ denotes ensemble averaging.

In Eq. 1 γ_i^λ depends on the oxide thickness d_λ^{ox} between the λ-lead and the nanoparticle. Within a simple parallel-plate capacitor model this thickness also determines the lead-dot capacitances $\mathcal{C}_T$ and $\mathcal{C}_B$ for leads T and B; for simplicity we assume $\mathcal{C}_T d_T^{ox} = \mathcal{C}_B d_B^{ox}$. Fig. 2 shows the calculated γ_i^λ , in units of $\Gamma_0 = 2\pi\mathcal{R}^2\nu_\lambda(E_H)/\hbar$ for the T and B surfaces, for the first few energy levels around the Fermi level for different capacitance ratios ($\mathcal{C}_B/\mathcal{C}_T = 1, 1.25$). We take as a reference $d_B^{ox} = 5\mathring{A}$ and $\kappa = 0.56\mathring{A}^{-1}$ [14]. When the thicknesses (capacitances) are equal, the tunneling efficiencies, although asymmetric, are of the same order of magnitude. As soon as the thickness (capacitance) ratio is changed *slightly* so that $d_B^{ox} < d_T^{ox}$, the asymmetry becomes stronger and γ_i^T falls rapidly by almost an order of magnitude relative to γ_i^B.

We calculate the electric current I through the nanoparticle and the differential conductance dI/dV assuming for simplicity that when an electron enters or leaves the nanoparticle the latter relaxes quickly to its electronic ground state. The complementary limit of slow relaxation has been studied previously [5,9], omitting however the new effects of charge fluctuations that we introduce here. We consider forward bias (FB) and reverse bias (RB) voltages V at which the electron population N of the nanoparticle changes by no more than ± 1 from its neutral value N_0. Thus the nanoparticle is neutral ($n = N - N_0 = 0$) or negatively ($n = 1$) or positively ($n = -1$) charged. We treat the electrostatic charging energy of the nanoparticle and leads according to standard Coulomb blockade theory [15]. We assume that at $V = 0$ the Fermi levels of the leads align with the highest occupied level of the neutral particle. The electrochemical potential of the $T(B)$ lead is $\mu^{T(B)} = E_F \pm eV\mathcal{C}_{B(T)}/\mathcal{C}_\Sigma$ with $\mathcal{C}_\Sigma = \mathcal{C}_T + \mathcal{C}_B$ [16]. The master equation for the population of the nanoparticle is then

$$\begin{aligned}
\partial_t n = \; & \delta_{n,0}\Big\{\textstyle\sum_i \gamma_i^T f(E_i + U - \mu^T)\sum_\sigma[1-\theta(E_i - E_F^\sigma)] - \sum_j \gamma_j^B[1 - f(E_j - U - \mu^B)]\sum_\sigma \theta(E_i - E_F^\sigma)\Big\} \\
& + \delta_{n,-1}\textstyle\sum_k[\gamma_k^T f(E_k - U - \mu^T) + \gamma_k^B f(E_k - U - \mu^B)]\sum_{\sigma,\sigma'}[1 - \theta(E_k - E_F^{\sigma,-\sigma'})] \\
& - \delta_{n,+1}\textstyle\sum_l\{\gamma_l^B[1 - f(E_l + U - \mu^B)] + \gamma_l^T[1 - f(E_l + U - \mu^T)]\}\sum_{\sigma,\sigma'}\theta(E_l - E_F^{\sigma,+\sigma'}) \\
& = \delta_{n,0}(\mathcal{S}_1^{T\to d} - \mathcal{S}_2^{d\to B}) + \delta_{n,-1}(\mathcal{S}_3^{T\to d} + \mathcal{S}_3^{B\to d}) - \delta_{n,+1}(\mathcal{S}_4^{d\to B} + \mathcal{S}_4^{d\to T}),
\end{aligned} \quad (2)$$

where the E_i are the one-electron energy levels of the neutral nanoparticle, $U = e^2/2\mathcal{C}_\Sigma$ is the single-electron charging energy [15], $f(x)$ is the Fermi distribution of the leads at temperature T_d and $\theta(x)$ is the Heaviside function describing the occupation of the levels in the nanoparticle. E_F^σ is the highest occupied level with spin $\sigma(=\uparrow,\downarrow)$. $E_F^{\sigma,-\sigma'}$ and $E_F^{\sigma,+\sigma'}$ denote the highest occupied level of the nanoparticle with spin σ after removal($-$) or addition($+$) of an electron with spin σ'. In Eq. 2 we assume FB with electron flow from T to B, therefore $\mu^T > \mu^B$. In RB the indices T and B are interchanged.

We now discuss the physical meaning of the terms in Eq. 2, keeping for the sake of clarity to the case $T_d = 0$. The sum over i in Eq. 2 describes processes in which an electron moves from lead T to the single-electron state $|\varphi_i\rangle$ of an initially neutral ($n = 0$) nanoparticle. This is allowed energetically if $E_i + U \le E_F + e\mathcal{C}_B V/\mathcal{C}_\Sigma$, i.e., the single-electron energy E_i of the level in the dot to which the transition is made plus the charging energy U must be lower than μ^T, the highest occupied level in the electrode. Also the single-particle state $|\varphi_i\rangle$ of the nanoparticle that accepts the electron, must be initially unoccupied. $f(x)$ and $\theta(x)$ with the arguments in Eq. 2 account for these constraints. Analogous reasoning leads to the other terms in Eq. 2. The sum over j describes tunneling from the neutral particle to electrode B which is allowed energetically if $E_j - U \ge \mu^B$. If the nanoparticle is *initially charged* different energetic restrictions apply: If $n = -1$ initially, tunneling from electrode $T(B)$ to the nanoparticle state $|\varphi_k\rangle$ is allowed if $E_k - U \le \mu^{T(B)}$. If $n = 1$ initially, an electron may tunnel from state $|\varphi_l\rangle$ of the nanoparticle to electrode $B(T)$ if $E_l + U \ge \mu^{B(T)}$.

The rate equations for the probability of the nanoparticle being in a given charge state ($n = -1, 0, +1$) are: $\partial_t P_1 = \mathcal{S}_1 P_0 - \mathcal{S}_4 P_1$, and $\partial_t P_{-1} = \mathcal{S}_2 P_0 - \mathcal{S}_3 P_{-1}$, with $P_0 + P_1 + P_{-1} = 1$. In *forward* bias the total rates are $\mathcal{S}_1 = \mathcal{S}_1^{T\to d}$, $\mathcal{S}_2 = \mathcal{S}_2^{d\to B}$, $\mathcal{S}_3 = \mathcal{S}_3^{T\to d} + \mathcal{S}_3^{B\to d}$, and $\mathcal{S}_4 = \mathcal{S}_4^{d\to B} + \mathcal{S}_4^{d\to T}$. We solve these rate equations for the steady state occupation probabilities P_n^{st}. Then the current $\mathcal{I}$ passing through the nanoparticle is

$$\mathcal{I}^{FB} = e(\mathcal{S}_1^{T\to d}P_0^{st} + \mathcal{S}_3^{T\to d}P_{-1}^{st} - \mathcal{S}_4^{d\to T}P_1^{st}). \quad (3)$$

Figure 3 shows our calculated differential conductance spectra for Al nanoparticles within the first step of the Coulomb staircase. The resonances labelled $i\lambda$ (λi) are due to tunneling from (to) level $|E_F + i\rangle$ of the *neutral* nanoparticle to (from) contact $\lambda = T, B$. Here $\bar{i} = -i$. We refer to these resonances as *neutral peaks* (NP). The other peaks labelled $Q^+(\bar{Q})$ are due to the $n = 1$ (-1) charge fluctuations on the nanoparticle that are induced by the current. They occur when a level of the charged nanoparticle (renormalized by the charging energy U) becomes available for transport as the electrochemical potentials of the contacts are swept. These resonances will be referred to as *charge fluctuation peaks* (CFP). Since on the first step of the Coulomb staircase the nanoparticle is neutral most of the time, most NP's are much stronger than most CFP's. However as will be explained below, some CFP's can be strongly enhanced by kinetic bottlenecks and thus become very prominent spectral features.

Another striking aspect of Fig. 3 is the strong tendency of the resonances to cluster that is also found experimentally [2]. To account for this clustering, previous theories [5,9] employed the *phenomenological* assumption that excited nanoparticle states are very long lived. Here we do *not* make this assumption; the clustering in Fig. 3 follows directly from our *microscopic* theory [10] of the electronic structure of the nanoparticle. Also in common with the experimental data [2] (but unlike the results of previous theories [5]) the amplitudes of the peaks in Fig. 3 show no systematic decrease with increasing bias V.

We now discuss the tunneling spectra in Fig. 3 in more detail. For FB we assume $\mu^T > \mu^B$ so the electrons flow from T to B. Note that the highest occupied level of the neutral nanoparticle is $i = 0$ and it is doubly occupied.

In Fig. 3a $\mathcal{C}_B = \mathcal{C}_T$ so the applied bias is divided equally between the two contacts. In FB the first resonance is $0B$ (tunneling from the $i = 0$ neutral nanoparticle level to lead B) and occurs at $V = 50\text{mV} = 2U/e$. This is followed at higher bias by other NP's interspersed with CFP's Q^+ and $\bar{Q}$. Since $\mathcal{C}_B = \mathcal{C}_T$ the spectrum under RB is similar with the roles of contacts T and B interchanged; each NP and CFP under FB has a counterpart *at the same voltage* under RB. The amplitudes of corresponding peaks under FB and RB are not identical because the calculated $\gamma_i^{T,B}$ are unequal; see Fig. 2a.

Experimentally, the B and T tunnel barriers have different thicknesses and hence unequal capacitances and very different tunneling efficiencies; see Fig. 2b. Fig. 3b shows such a case with $\mathcal{C}_B = 1.25\mathcal{C}_T$ which implies bias-induced changes in μ^T 1.25 times larger than those in μ^B. Thus corresponding NP's now occur at FB and RB values that differ by the capacitance ratio. For example, $0T$ is at 45mV in RB while its FB partner $0B$ is at 45mV$\times$1.25 =56mV. Despite the large asymmetry between γ_i^B and γ_i^T in Fig. 2b, the amplitudes of the NP's are quite similar under FB and RB in Fig. 3b because in each case the current must pass through *both* the T and B tunnel barriers. However for asymmetric tunnel barriers the amplitudes of the CFP's are very different under FB and RB: In Fig. 3b the $\bar{Q}$ CFP's are much stronger than the Q^+ CFP's under FB while the reverse is true under RB. *This is because asymmetric tunnel barriers affect the kinetics of positive and negative charge fluctuations differently*: A Q^+ charge fluctuation implies an electron surplus on the nanoparticle. Under FB this fluctuation dissipates easily to the drain (the B contact) since γ_i^B is large, thus the total current and dI/dV are affected little by the introduction of an additional decay channel and the Q^+ CFP's are weak. Conversely, a $\bar{Q}$ fluctuation (an electron deficit on the nanoparticle) does *not* dissipate as readily under FB since this requires tunneling from the source (T) contact through the weakly transmitting (T) barrier. Thus here the introduction of a new conducting channel has a larger effect on I and dI/dV and $\bar{Q}$ CFP's are strong in FB. Under RB the transport bottleneck is reversed and $\bar{Q}$ CFP's are weak while Q^+ CFP's are strong. Thus the new charge fluctuation resonances that we have introduced here readily account for the previously puzzling experimental tunneling features that have no identifiable partner when the bias is reversed. [2]

In conclusion, we have presented the first calculations of electron transport through metal nanoparticles that are based on a microscopic theory of their electronic structure. We have shown theoretically that charge fluctuations give rise to tunneling resonances of a new type that account for the behavior of previously unexplained spectral features that are observed experimentally.

This research has been funded by NSERC and CIAR.

[1] W. P. Halperin, Rev. Mod. Phys. **58**, 533 (1986); J. v. Delft and D. C. Ralph, Phys. Rep. **345**, 61 (2001).

[2] D. C. Ralph, C. T. Black, and M. Tinkham, Phys. Rev. Lett. **74**, 3241 (1995); Physica **218B**, 258 (1996)

[3] D. Davidović and M. Tinkham, Phys. Rev. Lett. **83**, 1644 (1999); Phys. Rev. B 61, R16359 (2000); J. R. Petta and D. C. Ralph, Phys. Rev. Lett. **87**, 266801 (2001)

[4] S. Guéron *et al.*, Phys. Rev. Lett. **83**, 4148 (1999); M. M. Deshmukh *et al.*, Phys. Rev. Lett. **87**, 226801 (2001)

[5] O. Agam, N. S. Wingreen, B. L. Altshuler, D. C. Ralph, and M. Tinkham, Phys. Rev. Lett. **78**, 1956 (1997)

[6] C. M. Canali and A. H. MacDonald, Phys. Rev. Lett. 85, 5623 (2000)

[7] S. Kleff, J. v. Delft, M. M. Deshmukh, and D. C. Ralph, Phys. Rev. B 64, 220401(R) (2001).

[8] I. L. Aleiner, P. W. Brouwer and L. I. Glazman, Phys. Rep. **358**, 309 (2002), and references therein.

[9] E. Bonet, M. M. Deshmukh, and D. C. Ralph, Phys. Rev. B**65**, 045317 (2002)

[10] G. A. Narvaez and G. Kirczenow, Phys. Rev. B**65**, 121403(R) (2002)

[11] S. P. McGlynn, L. G. Vanquickenborne, M. Kinoshita, D.

G. Carroll, *Introduction to Applied Quantum Chemistry* (Holt, Rinehart, Winston, New York, 1972)
[12] L. I. Schiff, *Quantum Mechanics* (McGraw-Hill, 1955)
[13] W. H. Rippard, A. C. Perrella, F. J. Albert, and R. A. Buhrman, Phys. Rev. Lett. **88**, 046805 (2002)
[14] Our results are qualitatively similar for $d_B^{ox} = 10\mathring{A}$.
[15] I. O. Kulik and R. I. Shekhter, Zh. Eksp. Teor. Fiz **68**, 623 (1975) (Sov. Phys.-JETP **41**, 308 (1975)); K. K. Likharev, IBM J. Res. Dev. **32**, 144 (1988); D. V. Averin and A. N. Korotkov, J. Low Temp. Phys **80**, 173 (1990);*ibid*, Zh. Eksp. Teor. Fiz **97**, 1661 (1990) (Sov. Phys.-JETP **70**, 1990); D. V. Averin and K. K. Likharev, in *Mesoscopic Phenomena in Solids*, Eds. B. L. Altshuler, P. A. Lee, and R. A. Webb, Elsevier, Amsterdam (1991).
[16] We include the bias voltage in this fashion because by *definition* eV is the difference between the electrochemical potentials in the leads at a given applied V.

FIG. 1. Energy levels near E_F (upper panel). Amplitude of φ_i at the T and B surface corresponding to the second level above (right) and below (left) the Fermi level (center). The second and third levels above the Fermi energy are nearly degenerate on this scale. $\delta^{Al} = (4E_F^{Al}/3\mathcal{N}^{Al})\mathcal{V}^{-1} = 5meV$. E_F^{Al} is the bulk Fermi energy and $\mathcal{N}^{Al}$ the electron density of Al.

FIG. 2. Tunneling efficiencies for energy levels $|E_F + i\rangle$ ($\bar{i} = -i$) for T and B leads.

FIG. 3. dI/dV in forward (FB) and reverse (RB) bias on a logarithmic scale; consecutive ticks indicate a decade. $U = 25$ meV, $T_d = 12$ mK; (a) $\mathcal{C}_B = \mathcal{C}_T$, (b) $\mathcal{C}_B = 1.25\mathcal{C}_T$. The inset is a detail of the structure indicated by *.

This figure "Fig1lanl.GIF" is available in "GIF" format from:

http://arXiv.org/ps/cond-mat/0207437v1

This figure "Fig2lanl.GIF" is available in "GIF" format from:

http://arXiv.org/ps/cond-mat/0207437v1

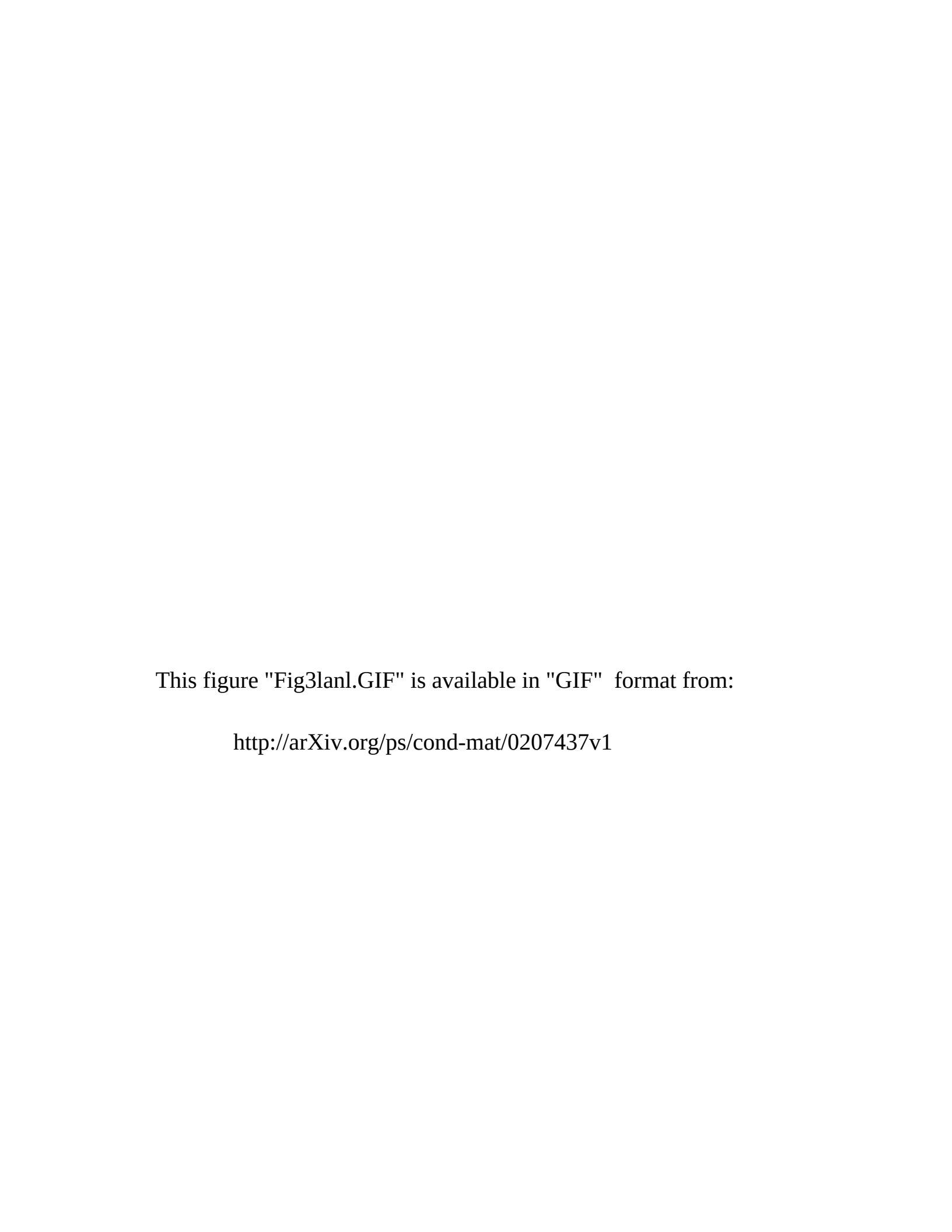
This figure "Fig3lanl.GIF" is available in "GIF" format from:
http://arXiv.org/ps/cond-mat/0207437v1